State reconstruction of molecular spatial rotation

Qin Xiao(覃 晓)[a)b)] and Gao Jun-Yi(高军毅)[a)†]

[a)] *Wuhan Institute of Physics and Mathematics, Chinese Academy of Sciences, Wuhan* 430071, *China*
[b)] *Graduate University of the Chinese Academy of Sciences, Beijing* 100049, *China*

(Received 19 May 2011; revised manuscript received 27 October 2011)

We establish a reconstruction approach for the rotational quantum state of linear molecules possessing a magnetic manifold. Our approximate method contains an iteration with generalized matrix inverses, processing the tomographic integral of the time-dependent molecular-axis distribution in a polar angle. As shown in a simulated example for an alignment state, the density matrix is determined in a high fidelity. An analytic tomographic formula is also derived for the symmetric top rotation. The state coherent in the quantum space of both the angular momentum and its magnetic projection can be approximately retrieved from the observable time-resolved solid-angle distribution of the molecular axis.

Keywords: state reconstruction, molecular rotation

PACS: 03.65.Wj, 33.20.Sn **DOI:** 10.1088/1674-1056/21/2/020303

1. Introduction

The issue to determine the state of a micro object from experimentally detectable quantities is significant in quantum physics. Various reconstruction approaches have been implemented on systems such as photons, atoms, and molecules (D'Ariano *et al.*[1] gave a review), and some methods have been proposed recently for larger scale systems.[2] An experimental frontier of this field is to reconstruct the molecular orbital (for the latest development the readers are referred to Ref. [3] for instance), even the transient electronic wavefunction during the tunneling ionization.[4]

The reconstruction of a molecular rotational state is enabled as the existence of non-adiabatic rotational excitation. Tasks such as the dynamical molecular alignment[5] prepare a field-free evolving coherent wavepacket detectable in experiments. The rotational state population has been decoded from a measure of rotational-level-resolved ionization.[6] Meanwhile, a pioneering method has been proposed by Mouritzen and Mølmer,[7] for a mixed state in the angular momentum space to be tomographically reconstructed from the time-dependent angular distribution. Imaging of a rigid-rotor state has also been numerically tested using the alternative observable of time-resolved orientation.[8] Then in a pure state case, rotational wavefunction of benzene molecule is determined through the ion-yield evolution of a single rotational level.[9]

In those earlier works, the object rotational state of linear and symmetric top molecules is confined specially in the angular momentum J space with a single magnetic projection M,[7,9,10] or the M subspace with a fixed J.[8] The generation of this type of rotation required a state-selective technique, such as the hexapole focusing, which might be tough in experiments. However, the rotational states populating in both the J and M dimensions are more familiar in nature. For example, the one-dimensional alignment of a thermal average ensemble[5] produces a state coherent in the J space within M manifold. Laser pulses of different polarizations lead to a planar alignment of molecules[11] and a unidirectional rotating wavepacket[12] where states coherent in both J and M are prepared.

Therefore, we focus on the reconstruction of the density matrix of a mixed rotational state, in the target space containing both the J and M dimensions. The observable time-dependent angular distribution of molecular axis in a simple pump-probe scheme is employed (a similar experiment refers to Ref. [13]). This measurable quantity, without the aid of rotational-state-resolved detection, provides as

†Corresponding author. E-mail: gaojunyi@wipm.ac.cn

© 2012 Chinese Physical Society and IOP Publishing Ltd

much knowledge as possible about the molecular rotation, yet is informationally incomplete.[14] Alternatively, we seek for an approximate solution by utilizing proper inverse methods, and the uniquely-determined part of the density matrix is specified through the tomographic integral. Major types of spatial rotation in this two-dimensional quantum space are examined in advance, and two cases are concluded applicable for our high-fidelity approximate reconstruction approach.

The organization of this paper is as follows. In Section 2 we establish an iterative reconstruction approach based on the structure of rotational level gaps, for the molecular rotation excited by a linearly polarized laser pulse. Configurations of this approach are shown, with an example of reconstruction, and the numerical character is investigated. Section 3 is devoted to the reconstruction of rotational states coherent in both the J and M spaces. A tomographic formula to retrieve the density matrix elements is deduced theoretically. The validity of our methods is discussed in the last section.

2. States of M manifold

A rotational state of linear molecules pumped by a source of linear polarization is coherent in J space. The nonzero density matrix element of this state is

$$\rho_{J_1MJ_2M} = \langle J_1M|\hat{\rho}|J_2M\rangle, \tag{1}$$

which is a rank-three target consisting of an M manifold. The density operator $\hat{\rho}$ as well as the density matrix is defined after the state preparation (noted as $t = 0$).

2.1. Angular distribution

The observable used in the reconstruction is the time-dependent molecular-axis angular distribution (TDMAAD), which could be obtained experimentally in a femtosecond laser pump-probe scheme with ion detection,[13] similar to the setup in Ref. [7] without prior magnetic-state selection. The expansion of TDMAAD in the spherical harmonics basis reads

$$R(\Omega,t) = \sum_{J_1J_2M} \exp\left(\frac{E_{J_1}-E_{J_2}}{i\hbar}t\right) \times \mathrm{Y}_{J_1M}(\Omega)\mathrm{Y}^*_{J_2M}(\Omega)\rho_{J_1MJ_2M}. \tag{2}$$

For molecular nitrogen thermally averaged at a temperature of 100 K, excited by a nonresonant 100-femtoseconds pulse of peak intensity 40 TW/cm^2, TDMAAD is calculated numerically (theory as Ref. [15]) and shown in Fig. 1.

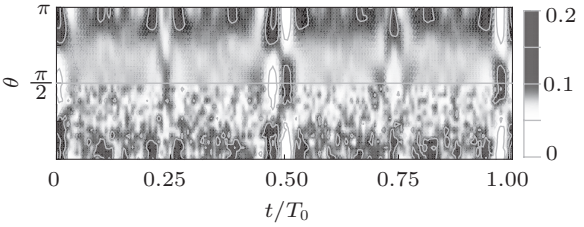


Fig. 1. The upper half $\theta \in [\pi/2, \pi]$ of the gray level plot shows the calculated TDMAAD sampled in the first rotational revival period $T_0 \simeq 8.35$ ps of N_2. The horizontal axis is the pump-probe delay and the vertical is the polar angle. The other half $\theta \in [0, \pi/2]$ illustrates the distribution with random Gaussian noise added on. The relative noise level here is $\eta = \frac{1}{5}$.

2.2. Tomographic integral

The first step is the tomographic integral of the TDMAAD, with the orthogonal kernel function of integer variables α and β. We have the following equation[10]

$$\begin{aligned} & S(\alpha,\beta) \\ &= \frac{1}{T_0}\int \mathrm{d}\Omega \int_0^{T_0} R(\Omega,t)\exp\left(-\frac{\pi\beta}{\mathrm{i}T_0}t\right)\mathrm{Y}_{\alpha 0}(\Omega)\,\mathrm{d}t \\ &= \sum_{J_1J_2M} \delta(\beta,\beta'_{J_1J_2})(-1)^M\sqrt{\frac{(2J_1+1)(2J_2+1)}{4\pi(2\alpha+1)}} \\ &\quad \times \langle J_1MJ_2-M|\alpha 0\rangle\langle J_10J_20|\alpha 0\rangle\rho_{J_1MJ_2M}. \end{aligned} \tag{3}$$

The Kronecker delta function is available under the rigid rotor approximation, and $\beta'_{J_1J_2} = J_1(J_1+1) - J_2(J_2+1)$. Separation of density matrix elements is provided by the delta function and the C-G coefficient[16] $\langle J_10J_20|\alpha 0\rangle$. For the sake of convenience, we still redefine the term degeneration for level pairs noted as $\{J_1, J_2\}$ that has an equivalent frequency $\beta'_{J_1J_2}$ and the same parity of $J_1 + J_2$, without concern for the energy degeneration of the magnetic states. For more details of the above theoretical frame refer to our earlier paper.[10]

2.3. Iterative matrix inverse

An iterative approach is constructed to handle the tomographic integral, using different matrix inverses dependent on the degeneration conditions of density matrix elements. In a non-degenerate circumstance (the degeneracy is equal to one), only one pair

$\{J_1, J_2\}$ corresponds to a certain β and single parity $J_1 + J_2$, so only the M sum survives in Eq. (3). Due to the equal initial population and transition moment, there is a symmetry $\rho_{J_1-MJ_2-M} = \rho_{J_1MJ_2M}$ to reduce the relevant set of elements to the vector $\boldsymbol{\rho} = \{\rho_{J_1MJ_2M}\}_{M\in[0,J_1]}$ of length $J_1 + 1$, assumed $J_1 < J_2$ without loss of generality. Meanwhile, the available number of $S(\alpha, \beta'_{J_1J_2})$ is also $J_1 + 1$ since α is constrained by the C-G coefficient. Listing the expression (3) as $\boldsymbol{S} = \{S(\alpha, \beta'_{J_1J_2})\}_{\alpha=[J_2-J_1,J_2-J_1+2,\cdots,J_2+J_1]}$, we have $\boldsymbol{S} = \Gamma \cdot \boldsymbol{\rho}$ with the numerical integral data at the left-hand side. The square coefficient matrix Γ is full rank due to the orthogonality of spherical harmonics, so a unique solution is given by the matrix inverse $\boldsymbol{\rho} = \Gamma^{-1} \cdot \boldsymbol{S}$.

Low-degree multiple degeneration relates to the degenerate off-diagonal elements. These cases are usually the minority in the density matrix (will be discussed in the last section). In such a multiple degeneration, since the number of degenerate elements is larger than the length of available $\boldsymbol{S}$, they cannot be uniquely determined only from TDMAAD. Formally $\boldsymbol{S} = \Gamma \cdot \boldsymbol{\rho}$ is written, but now Γ is rectangle. The regular minimum norm solution is picked out at first, i.e. $\boldsymbol{\rho} = \Gamma^+ \cdot \boldsymbol{S}$ with Γ^+ the Moore–Penrose pseudoinverse.[17] As the degeneracy for $J_1 \neq J_2$ is often small, this solution is already a good approximation to the "true" value of the object state.

The largest degeneracy relates to all the diagonal elements $\boldsymbol{\rho} = \{\rho_{JMJM}\}$, where $M \in [0, J]$ and $J \in [0, J_{\max}]$. The number of these indeterminant is $\sum_{J=0}^{J_{\max}}(J + 1) = (J_{\max} + 1)(J_{\max} + 2)/2$, and $J_{\max}$ is the artificial upper cutoff in the angular momentum space. In the meantime, valid constrain is $\boldsymbol{S} = \{S(\alpha, 0)\}_{\alpha\in[0,2J_{\max}]}$ for even α, with length only $J_{\max} + 1$. For an ordinary cutoff, this situation is always extremely under-determined. Nonetheless, a weighted generalized inverse[18] is founded. According to the Schwartz inequality $|\rho_{J_1MJ_2M}| \leq (\rho_{J_1MJ_1M} \times \rho_{J_2MJ_2M})^{1/2}$, a factor $w_{JMJM} = (|\rho_{JM(J+\Delta J)M} \times \rho_{JM(J-\Delta J)M}|)^{1/2}$ is appointed for each diagonal element. A nonzero ΔJ is selected based on the chiefly occupied off-diagonal elements, and the dominant Raman transition of this state decides $\Delta J = 2$ here. The positive weighted diagonal matrix is $N = \mathrm{Diag}\{w_{JMJM}\}$, where the order of J and M is the same as $\boldsymbol{\rho}$. Then the generalized inverse is $\Gamma_N^+ = N^{1/2}(\Gamma N^{1/2})^+$, and the weighted minimum norm solution for diagonal elements is $\boldsymbol{\rho} = \Gamma_N^+ \cdot \boldsymbol{S}$.

A total density matrix is obtained, but a single iteration is implemented as an improvement. Now the multiply degenerate off-diagonal elements are retrieved by a weighted inverse instead of the regular minimum norm inverse, and the weight $w_{J_1MJ_2M} = (|\rho_{J_1MJ_1M} \times \rho_{J_2MJ_2M}|)^{1/2}$ is produced from the retrieved diagonal elements. Then if some off-diagonal elements with indexes $J_1 - J_2 = \Delta J$ are multiply degenerate, the weights of the inverse for diagonals are refreshed, and the diagonal elements are retrieved again. The solution set here is expected to exhibit a better physical property.

2.4. Example of an alignment state

The reconstruction result from the data in Fig. 1 is shown in Fig. 2. With the chosen cutoff $J_{\max} = 14$, it is checked that most of the density matrix elements are non-degenerate. There are only 44 pairs of $\{J_1, J_2\}$ are doubly degenerate. Degeneracy larger than 2 is just the case of diagonal elements. Consequently, the majority of the elements are directly extracted from the TDMAAD.

Examined by sampling without noise (Fig. 2(b)), non-degenerate elements are precisely reconstructed. The weighted minimum norm solution brings in some error for occupied degenerate off-diagonals, while major discrepancy appears in diagonal elements. Nonetheless, the profile for each M block is mimicked and a reconstruction fidelity $O \sim 0.97$ is reached in this situation. Here the fidelity is defined following Ref. [10] that

$$O = \mathrm{tr}[\hat{\rho}_{\mathrm{pre}} \cdot \hat{\rho}_{\mathrm{rec}}]/(\mathrm{tr}[\hat{\rho}_{\mathrm{pre}}^2]\,\mathrm{tr}[\hat{\rho}_{\mathrm{rec}}^2])^{1/2}.$$

In the noisy condition, fluctuations exist in the density matrix, see Fig. 2(c). The degenerate elements appear to gain more error, since the weighted factors are also distorted. A low noise level here $\eta = \frac{1}{5}$ produces relatively large error to elements of small amplitude. Reconstruction fidelity goes down to $O \sim 0.87$, indicating the strict requirement on the precision of such an experiment. As a comparison, the error coming from the approximations of the method is fairly small in this example.

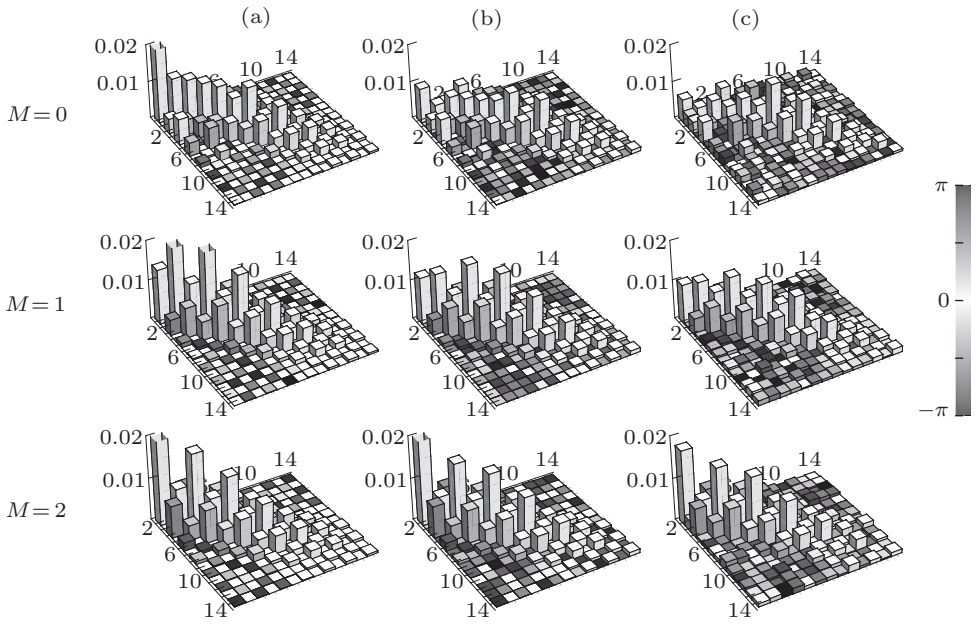


Fig. 2. Magnetic diagonal blocks of the density matrix $\langle J_1 M|\hat{\rho}|J_2 M\rangle$ with $M = 0, 1, 2$ are plotted. The two integer coordinates for each block are J_1 and J_2, respectively. The left row (a) is the prediction from quantum mechanic calculation. This broad distributed alignment state exhibits strong coherence in $\Delta J = \pm 2$. Rows (b) and (c) are the results of reconstruction from data without and with artificial noise, respectively. The quantum phase of each element is represented in gray level, scaled in the right side.

2.5. Convergence and numerical stability

The convergence here refers to whether a single density matrix is definitely received, while the "true" state cannot be found due to the informational incompleteness. This convergence is identified in the noiseless condition (full line in Fig. 3), as the increase of the angular momentum cutoff. The fidelity rises to a constant near unity, which means the reconstructed state is a good imitation of the target.

When artificial noise is contained, the reconstruction shows its best performance around $J_{\max} = 12$ (dashed line in Fig. 3). As a single wavepacket, components of higher angular momentum mainly receive noise in the reconstruction, which leads to a growing discrepancy. In a random noise condition, a proper cutoff could be chosen by judging, e.g., whether the diagonal elements at the edge $\rho_{J_{\max}MJ_{\max}M}$ have random behavior as $J_{\max}$ increases (the $J_{\max} = 14$ in the example is chosen in this manner), or significantly less than a predicted noise level.

The matrix inverses are non-orthogonal transforms, in which numerical stability should be examined. As to the perturbation $\delta\boldsymbol{S}$ transferred from the noise of the TDMAAD, there is a limit $|\delta\boldsymbol{\rho}| \leq ||\Gamma^+|| \times |\delta\boldsymbol{S}|$ for the matrix inverse. Here Γ^+ represents universally any coefficient matrix inverse used in the reconstruction, and its norm denotes the amplification factor of the perturbation. $||\Gamma^+|| = 1/\sigma_{\min}(\Gamma)$ is just the reciprocal of the minimal singular value of the matrix.[18] The maximum of this norm among all the employed inverses is illustrated in Fig. 3. It is found that the value begins at $2\sqrt{\pi}$ for $J_{\max} = 0$, showing a normal amplification factor of the non-unitary transform, while it slightly goes up to a bound $\sqrt{2}\pi$ as the increase of $J_{\max}$. The rate of enhancement is about

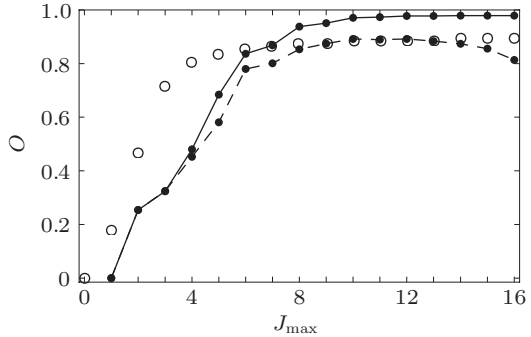


Fig. 3. The reconstruction fidelity is shown as a function of angular momentum cutoff. Reconstructions from data without and with noise are marked with full circles connected by full and dashed lines, respectively. These curves are received by treating the data in Fig. 1, with the sampling density varied according to $J_{\max}$. Each open circle is the maximal value of $||\Gamma^+||$ among all the matrix inverses employed for a certain $J_{\max}$, subtracting the minimum $2\sqrt{\pi}$.

1.25 at most, which indicates that these inverses are quite stable to noise perturbation, in consistent with the simulated result.

3. States coherent in both the J and M spaces

The universal spatial rotation of the molecular axis corresponds to a coherent mixed state in the two-dimensional J and M quantum spaces. This state can be produced for molecules excited by arbitrarily polarized short pulses, see e.g. Refs. [11], [12], and [19]. For these rotational states of symmetric top molecules, a tomographic reconstruction approach is established in the following. The eigenstate of this species is the rotation matrix function[20] in Euler angle space

$$\langle \Omega | JKM \rangle = \sqrt{\frac{2J+1}{8\pi^2}} D^{J*}_{MK}(\Omega),$$

with K the projection of J along the major principal molecular axis, denoting the self-rotation around this symmetric axis.

3.1. Description of state and observable

Assume an object state with selected single $K = K_0$ is prepared, and this quantum number is conserved in the laser excitation for symmetric top molecules. The general Raman transition rule is $\Delta J = 0, \pm 1, \pm 2$, and $\Delta M = 0, \pm 2$.[9] The rank-four density matrix in the angular momentum basis is

$$\rho_{J_1 M_1 J_2 M_2} = \langle J_1 K_0 M_1 | \hat{\rho} | J_2 K_0 M_2 \rangle, \tag{4}$$

where the conserved K_0 index is ignored in the abbreviation.

The distribution of molecular axis might be inhomogeneous in both the polar and azimuthal angles due to the state coherence, yet homogeneous in the Euler angle of the self-rotation. The molecular spatial orientation can be detected by using a slice imaging device.[21] Time-resolved pump-probe scheme is maintained, and the observable TDMAAD now is three-dimensional

$$\begin{aligned} R(\Omega, t) = & \sum_{J_1 M_1 J_2 M_2} \frac{\sqrt{(2J_1+1)(2J_2+1)}}{8\pi^2} \\ & \times D^{J_1 *}_{M_1 K_0}(\Omega) D^{J_2}_{M_2 K_0}(\Omega) \\ & \times \exp\left(\frac{E_{J_1} - E_{J_2}}{\mathrm{i}\hbar} t \right) \rho_{J_1 M_1 J_2 M_2}. \end{aligned} \tag{5}$$

To maximally record the evolution, the full solid angle with the pump-probe delay varied in one rotational revival period $T_0 \sim 1/2B$ should be covered, where B is the rotational constant perpendicular to the rotationally symmetric axis of the molecule. The energy of a symmetric-top rigid rotor is $E(J,K) = BJ(J+1) + (C-B)K^2$ abbreviated as E_J for a single K_0, and C is the rotational constant along the symmetric axis.[20]

3.2. Tomographic reconstruction

The projection of TDMAAD to an orthogonal basis is kept

$$\begin{aligned} & S(\alpha, \beta, \varepsilon) \\ = & \frac{1}{T_0} \int \mathrm{d}\Omega \int_0^{T_0} R(\Omega, t) \\ & \times \exp\left(-\frac{\pi\beta}{\mathrm{i}T_0} t \right) \sqrt{\frac{2\alpha+1}{8\pi^2}} D^{\alpha}_{\varepsilon 0}(\Omega) \mathrm{d}t. \end{aligned} \tag{6}$$

An additional variable $\varepsilon \in [-\alpha, \alpha]$ denotes the integer magnetic projection of α. With Eq. (5) substituted, the integral over the Euler angle is simplified by the coupling property of the $D^J_{MK}(\Omega)$ function,[16] and gives

$$\begin{aligned} & S(\alpha, \beta, \varepsilon) \\ = & \sum_{J_1 M_1 J_2 M_2} \delta(\beta, \beta'_{J_1 J_2}) (-1)^{M_2 + K_0} \\ & \times \sqrt{\frac{(2J_1+1)(2J_2+1)}{8\pi^2(2\alpha+1)}} \\ & \times \langle J_1 M_1 J_2 - M_2 | \alpha\varepsilon \rangle \langle J_1 K_0 J_2 - K_0 | \alpha 0 \rangle \\ & \times \rho_{J_1 M_1 J_2 M_2}. \end{aligned} \tag{7}$$

The delta function still comes from the Fourier-type transform.

A weighted sum of the tomographic integral is introduced

$$\begin{aligned} & h(J_1, M_1, J_2, M_2) \\ = & \sum_{\alpha\varepsilon} (-1)^{M_2 + K_0} \sqrt{\frac{8\pi^2(2\alpha+1)}{(2J_1+1)(2J_2+1)}} \\ & \times \frac{\langle J_1 M_1 J_2 - M_2 | \alpha\varepsilon \rangle}{\langle J_1 K_0 J_2 - K_0 | \alpha 0 \rangle} S(\alpha, \beta'_{J_1 J_2}, \varepsilon), \end{aligned} \tag{8}$$

analogous to the case of spin tomography,[22] and the range of α as well as ε is constrained by the C-G coefficient. This formula requires a nonzero denominator $\langle J_1 K_0 J_2 - K_0 | \alpha 0 \rangle$ for each α within the triangle rule, which is normally ensured by $K_0 \neq 0$. Elements degenerate if they own the same $\beta'_{J_1 J_2}$, and it is noted that for nonzero K_0 the separation by the

parity of $J_1 + J_2$ vanishes, see Eq. (7). Nevertheless, non-degenerate cases are still the majority in the density matrix.

By the substitution of Eq. (7), the following expression is received

$$\begin{aligned} & h(J_1, M_1, J_2, M_2) \\ = \; & \rho_{J_1 M_1 J_2 M_2} \\ & + \sum_{\alpha\varepsilon J_3 M_3 J_4 M_4} \delta(\beta'_{J_3 J_4}, \beta'_{J_1 J_2})(-1)^{M_2+M_4} \\ & \times \sqrt{\frac{(2J_3+1)(2J_4+1)}{(2J_1+1)(2J_2+1)}} \frac{\langle J_1 M_1 J_2 - M_2 | \alpha\varepsilon\rangle}{\langle J_1 K_0 J_2 - K_0 | \alpha 0\rangle} \\ & \times \langle J_3 M_3 J_4 - M_4 | \alpha\varepsilon\rangle \langle J_3 K_0 J_4 - K_0 | \alpha 0\rangle \\ & \times \rho_{J_3 M_3 J_4 M_4}. \end{aligned} \tag{9}$$

The first single term is obtained through the summation orthogonality of C-G coefficients,[16] and the sum over $\{J_3, J_4\}$ in the second term is the possible degeneration to $\{J_1, J_2\}$.

An approximate solution of the state will be given from those equations, provided the integral (6) has been numerically calculated for each valid set of $\{\alpha, \beta, \varepsilon\}$. Concerning a non-degenerate pair $\{J_1, J_2\}$, only the first term survives in the right-hand side of Eq. (9). Elements of this case are straightly retrieved by calculating the sum (8), with variable $\{M_1, M_2\}$. In multiple degenerations, elements of $\beta'_{J_3 J_4} = \beta'_{J_1 J_2}$ and $M_3 - M_4 = M_1 - M_2$ coexist in Eq. (9). As the number of independent constrains is insufficient, the elements cannot be solved by the equation system founded by the entire set of $S(\alpha, \beta, \varepsilon)$, or $h(J_1, M_1, J_2, M_2)$. Formally, $h(J_1, M_1, J_2, M_2)$ seems one-to-one mapped to $\rho_{J_1 M_1 J_2 M_2}$ as a rough solution, but the sum over the degeneration cannot be generally ignored in this informationally incomplete case. For those degenerate elements, the iterative generalized inverse approach in Section 2 is suggested, seeking for a weighted minimum norm solution. In general, these minority elements are only expected to induce a secondary influence to the reconstruction fidelity.

4. Discussion and conclusion

The method proposed in Section 2 aims at the reconstruction of quantum states prepared in strong-field rotational excitation, particularly the nonadiabatic alignment of linear molecules.[5] Despite TDMAAD being informationally incomplete for states of multiple magnetic number, the approach is efficient by considering the natural symmetry of rotation, and the few-degeneration structure of the temporal frequencies. Due to the even density of rotational state in energy space, the few-degeneration feature is independent of the angular momentum cutoff. This intrinsic property indeed reveals the universality for both of our approaches. Besides, the unique solution is selected from an infinite compatible set, and the weighted inverse based on Schwartz inequality is reasonable because of the coherence of the object state. Nonetheless, as the general broad spread of the alignment wavepacket, favorable reconstruction is only expected from a high-precision measurement. Specifically, the experimental ion images[5,13] must be Abel invertible with small error.

Concerning the state coherent in both J and M spaces, the tomographic approach is valid when the rotation is confined in a subspace of $K_0 \neq 0$, which excludes linear molecules, e.g., the states in Refs. [11] and [19]. A nonzero K_0 state for symmetric top molecules might be produced in a hexapole device,[23] and then could be excited by short pulses of arbitrary polarization. Detection using slice imaging[21] to receive a two-dimensional angular distribution with good statistics will be quite difficult, especially consuming in such a delay-varying collection. The complexities in both the state preparation and measurement have restrained the application of this method.

In principle, the reconstruction strategy of maximum likelihood[24] offers a statistically more reliable determination than the mathematical inverse. However, for an object density matrix of such a large scale, the numerical maximization will probably fail. The solution set is also infinite regarding this informationally incomplete problem. Nonetheless, the maximum likelihood strategy using a parameterized simple model of the target is an option especially for diagonal elements.

In conclusion, we developed approximate reconstruction approaches to retrieve the rotational state in two cases. For linear rotor states coherent in J space, the generalized inverse provides a high fidelity solution. The approach is proved numerically converged and is well-conditioned. Then, concerning symmetric top rotation with nonzero single K_0, the tomographic reconstruction gives an analytic form to non-degenerate elements. In principle, for general states in J and M spaces, complete information would be supplied by observables of higher rank, e.g. the rotational-state-resolved detection.[6] Considering

its challenging experimental realization, our methods serve as a good alternative due to its simplicity.

References

[1] D'Ariano G M, Paris M G A and Sacchi M F 2003 *Adv. Imag. Elect. Phys.* **128** 205

[2] Cramer M, Plenio M B, Flammia S T, Somma R, Gross D, Bartlett S D, Landon-Cardinal O, Poulin D and Liu Y K 2010 *Nature Commun.* **1** 149

[3] Vozzi C, Negro M, Calegari F, Sansone G, Nisoli M, de Silvestri S and Stagira S 2011 *Nature Phys.* **7** 822

[4] Haessler S, Caillat J, Boutu W, Giovanetti-Teixeira C, Ruchon T, Auguste T, Diveki Z, Breger P, Maquet A, Carré B, Taïeb R and Salières P 2010 *Nature Phys.* **6** 200

[5] Rosca-Pruna F and Vrakking M J J 2001 *Phys. Rev. Lett.* **87** 153902

[6] Hasegawa H and Ohshima Y 2006 *Phys. Rev.* A **74** 061401

[7] Mouritzen A S and Mølmer K 2006 *J. Chem. Phys.* **124** 244311

[8] Deshpande S A and Ezra G S 2007 *Chem. Phys. Lett.* **440** 341

[9] Hasegawa H and Ohshima Y 2008 *Phys. Rev. Lett.* **101** 053002

[10] Qin X and Gao J Y 2011 *Chin. Phys.* B **20** 010306

[11] Hoque Md Z, Lapert M, Hertz E, Billard F, Sugny D, Lavorel B and Faucher O 2011 *Phys. Rev.* A **84** 013409

[12] Kitano K, Hasegawa H and Ohshima Y 2009 *Phys. Rev. Lett.* **103** 223002

[13] Dooley P W, Litvinyuk I V, Lee K F, Rayner D M, Spanner M, Villeneuve D M and Corkum P B 2003 *Phys. Rev.* A **68** 023406

[14] Busch P 1991 *Int. J. Theor. Phys.* **30** 1217

[15] Rosca-Pruna F and Vrakking M J J 2002 *J. Chem. Phys.* **116** 6579

[16] Varshalovich D A, Moskalev A N and Khersonskii A K 1988 *Quantum Theory of Angular Momentum* (Singapore: World Scientific) pp. 72–117, 130–163, 235–270

[17] Rao C R and Mitra S K 1972 *Proceedings of the Sixth Berkeley Symposium on Mathematical Statistics and Probability* Vol. 1 Berkeley, United States of America, 1970 pp. 601–620

[18] Ben-Israel A and Greville T N E 2003 *Generalized Inverse Theory and Applications* 2nd edn. (New York: Springer-Varlag) pp. 102–104, 182–184

[19] Daems D, Guérin S, Hertz E, Jauslin H R, Lavorel B and Faucher O 2005 *Phys. Rev. Lett.* **95** 063005

[20] Gordy W and Cook R L 1984 *Microwave Molecular Spectra* 3rd edn. (New York: Wiley Interscience) pp. 11–35

[21] Gebhardt C R, Rakitzis T P, Samartzis P C, Ladopoulos V and Kitsopoulos T N 2001 *Rev. Sci. Instrum.* **72** 3848

[22] Manko V I and Manko O V 1997 *J. Exp. Theor. Phys.* **85** 430

[23] Anderson R W 1997 *J. Phys. Chem.* A **101** 7664

[24] Banaszek K, D'Ariano G M, Paris M G A and Sacchi M F 2000 *Phys. Rev.* A **61** 010304